

[Supplementary Material] Blind Non-Uniform Motion Deblurring using Atrous Spatial Pyramid Deformable Convolution and Deblurring-Reblurring Consistency

Dong Huo, Abbas Masoumzadeh, Yee-Hong Yang
 Department of Computing Science
 University of Alberta, Edmonton, Canada
 {dhuo, a.masoumzadeh, herberty}@ualberta.ca

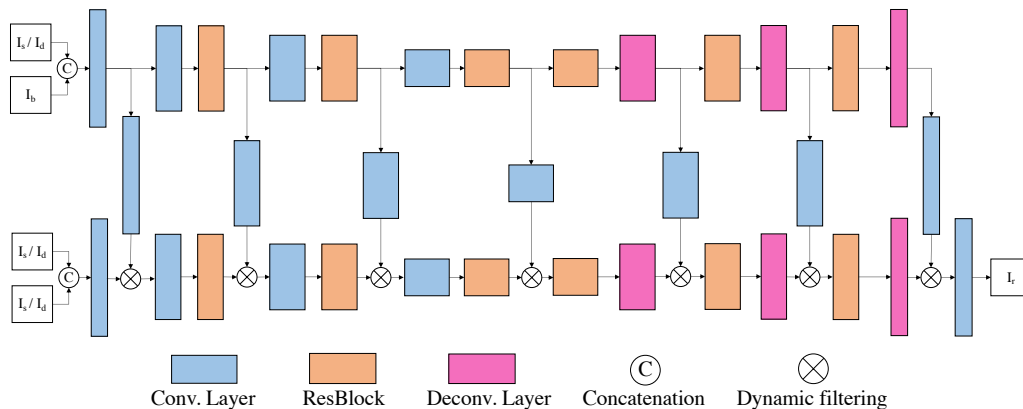


Figure 1. Detailed architecture of the reblurring network.

1. Reblurring Network

The detailed architecture of the reblurring network is shown in Fig. 1. Feature maps of the upper branch are passed to a convolution layer to generate dynamic local filters for the lower branch, *i.e.* the spatial-variant blur kernels. Then the feature maps of the lower branch are gradually reblurred until the final reblurred outputs. The parameters of upper and lower branches are shared.

2. More Qualitative Comparison

In this section, we demonstrate more qualitative comparisons. Firstly, we look at the GoPro dataset [2]. In Figure 2, Ours+ can recover the face and the body of the girl with less distortion. In Figure 3, the original image contains extremely large motion, but Ours+ can remove most of the artifacts and obtain the sharpest image among the listed methods. In Figure 4, Ours+ can recover clearer and smoother numbers on the plate.

Using the models trained on the GoPro dataset, we also compare the qualitative performance of the methods on the HIDE dataset [5], containing multiple moving human subjects in the scenes. In Figure 5, Ours+ sharpens all the peo-

ple in the image with much less artifacts compared to the other competing methods. Figure 6 shows that Ours+ deblurs the striped jacket closest to that of the ground truth. In Figure 7, Ours+ provides a relatively better deblurring of the car when compared with the other methods.

Lastly, we review some outputs from the Real-World Blurred Image (RWBI) dataset [8]. In Figure 8, Ours+ is the only method that gives sharp output for both the Starbucks logo and the tree leaves that are close to the camera. In Figure 9, only Ours+ and DeblurGANv2 [1] deblur the letters written on the wall. However, DeblurGANv2 fails to deblur the grass. In Figure 10, Ours+ can recover the poster on the background with the highest quality.



(a) Blurred input

(b) Kupyn [1]



(c) Zhang [7]



(d) Tao [6]



(e) Park [3]



(f) Prohit [4]



(g) Ours+



(h) Sharp GT

Figure 2. Qualitative comparison using the GoPro dataset [2].



(a) Blurred input



(b) Kupyn [1]



(c) Zhang [7]



(d) Tao [6]



(e) Park [3]



(f) Prohit [4]



(g) Ours+



(h) Sharp GT

Figure 3. Qualitative comparison using the GoPro dataset [2].



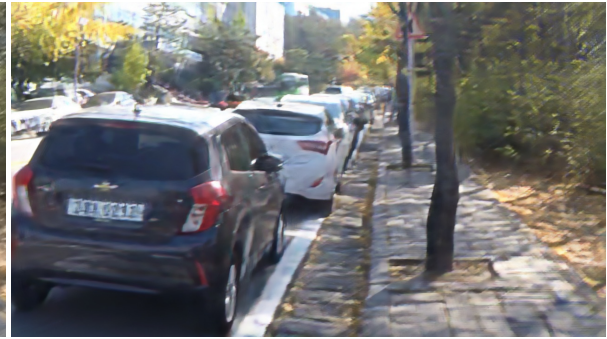
(a) Blurred input



(b) Kupyn [1]



(c) Zhang [7]



(d) Tao [6]



(e) Park [3]



(f) Prohit [4]



(g) Ours+



(h) Sharp GT

Figure 4. Qualitative comparison using the GoPro dataset [2].



(a) Blurred input



(b) Kupyn [1]



(c) Zhang [7]



(d) Tao [6]



(e) Park [3]



(f) Ours+



(g) Sharp GT

Figure 5. Qualitative comparison using the HIDE dataset [5].



(a) Blurred input



(b) Kupyn [1]



(c) Zhang [7]



(d) Tao [6]



(e) Park [3]



(f) Ours+



(g) Sharp GT

Figure 6. Qualitative comparison using the HIDE dataset [5].



(a) Blurred input



(b) Kupyn [1]



(c) Zhang [7]



(d) Tao [6]



(e) Park [3]



(f) Ours+



(g) Sharp GT

Figure 7. Qualitative comparison using the HIDE dataset [5].

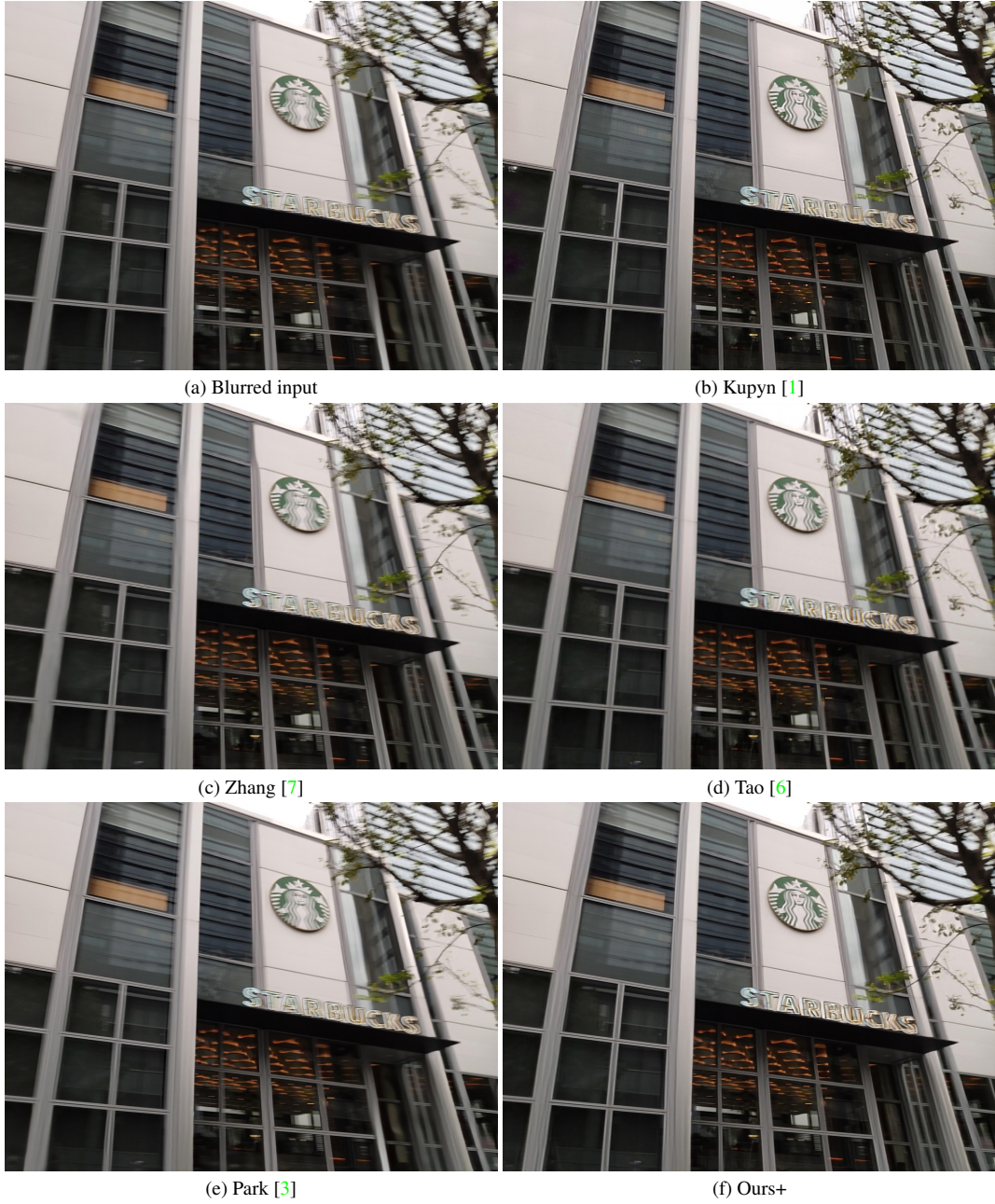


Figure 8. Qualitative comparison using the RWBI dataset [8].



Figure 9. Qualitative comparison using the RWBI dataset [8].

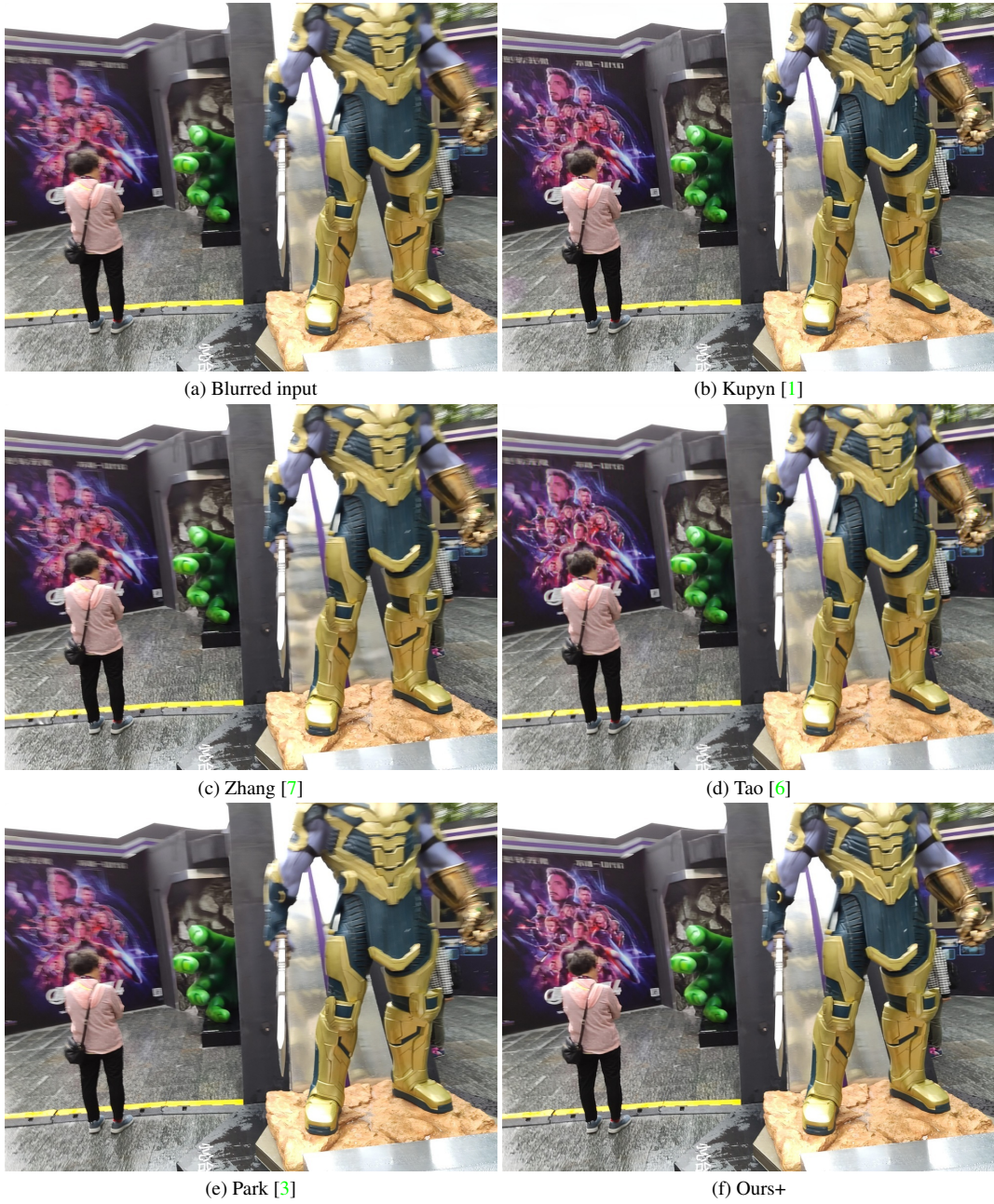


Figure 10. Qualitative comparison using the RWBI dataset [8].

References

- [1] Orest Kupyn, Tetiana Martyniuk, Junru Wu, and Zhangyang Wang. Deblurgan-v2: Deblurring (orders-of-magnitude) faster and better. In *ICCV*, 2019. [1](#), [2](#), [3](#), [4](#), [5](#), [6](#), [7](#), [8](#), [9](#), [10](#)
- [2] Seungjun Nah, Tae Hyun Kim, and Kyoung Mu Lee. Deep multi-scale convolutional neural network for dynamic scene deblurring. In *CVPR*, 2017. [1](#), [2](#), [3](#), [4](#)
- [3] Dongwon Park, Dong Un Kang, Jisoo Kim, and Se Young Chun. Multi-temporal recurrent neural networks for progressive non-uniform single image deblurring with incremental temporal training. In *ECCV*, 2020. [2](#), [3](#), [4](#), [5](#), [6](#), [7](#), [8](#), [9](#), [10](#)
- [4] Kuldeep Purohit and AN Rajagopalan. Region-adaptive dense network for efficient motion deblurring. In *AAAI*, 2020. [2](#), [3](#), [4](#)
- [5] Ziyi Shen, Wenguan Wang, Xiankai Lu, Jianbing Shen, Haibin Ling, Tingfa Xu, and Ling Shao. Human-aware motion deblurring. In *ICCV*, 2019. [1](#), [5](#), [6](#), [7](#)
- [6] Xin Tao, Hongyun Gao, Xiaoyong Shen, Jue Wang, and Jiaya Jia. Scale-recurrent network for deep image deblurring. In *CVPR*, 2018. [2](#), [3](#), [4](#), [5](#), [6](#), [7](#), [8](#), [9](#), [10](#)
- [7] Hongguang Zhang, Yuchao Dai, Hongdong Li, and Piotr Koniusz. Deep stacked hierarchical multi-patch network for image deblurring. In *CVPR*, 2019. [2](#), [3](#), [4](#), [5](#), [6](#), [7](#), [8](#), [9](#), [10](#)
- [8] Kaihao Zhang, Wenhan Luo, Yiran Zhong, Lin Ma, Bjorn Stenger, Wei Liu, and Hongdong Li. Deblurring by realistic blurring. In *CVPR*, 2020. [1](#), [8](#), [9](#), [10](#)